Solid Freeform Fabrication 2023: Proceedings of the 34th Annual International Solid Freeform Fabrication Symposium – An Additive Manufacturing Conference
Reviewed Paper

Novel Concepts to Integrate Dense and Sparse Infill Regions in Material Extrusion AM Parts

Logan J. Hutton*, Joseph Bartolai*
*Department of Mechanical Engineering, The Pennsylvania State University

Abstract

Modern toolpath generation softwares, or “slicers," allow for multiple regions within a Material Extrusion Additive Manufacturing produced part to be assigned different processing parameters, including infill density. Contemporary slicers develop these different infill regions independently, leading to discontinuities in the toolpaths at the region's boundaries. This work investigates the effect these discontinuities have on part strength, and tests a variety of novel approaches to connect infill regions in a continuous manner to improve part properties. Mechanical properties of parts built by toolpaths generated using Ultimaker Cura and Slic3r are compared to those of parts built using the novel build strategies presented in this work. The continuous and sequential novel build strategies presented in this work show statistically significant mechanical property increases.

Introduction & Prior Work

Material extrusion (MEX) additive manufacturing (AM) slicers have the ability to change printing parameters for any number of defined regions within a part [1,2]. The most common use for defining one of these regions is to define sections of sparse and dense infill to strategically strengthen or lighten the as-built part. When parameters that directly affect the toolpath are changed in one of these regions, the slicer will independently develop the toolpaths for each region. This leads to the part being built as if it was multiple parts on the build plate that just happen to be touching one another. The boundaries of these adjacent regions are not printed sequentially, leading to a large temperature difference between the road being extruded and the previously extruded road.

The temperature difference between adjacent roads at the boundaries of these regions can lead to poor bonding between the roads and a weak spot in the part [3–6]. These defects severely limit the use case of defining regions of varying parameters in a single part. Defining a region of dense infill at a high stress region in a part does not significantly increase the strength of the region, due to the defects at the boundary of the dense infill region [3].

There have been various studies on how infill patterns and density affect the final part strength. Yadav et al. and separately Abbas et al. specifically looked at compressive strength of various infill patterns and found that the compressive strength of all tested infill patterns increased with infill percentage [7,8]. A study of infill parameters effect on tensile strength was produced by Panzdzic et al. and found that ultimate and yield strength increase with infill density for every infill pattern tested [9]. The orientation of the part as printed and therefore the orientation of the infill as printed has a dramatic effect on part strength [10]. Varying the infill pattern and percentage on a layer basis to optimize the strength and weight of a part was studied by Dave et al [11]. It was found that at lower infill density strength of the part can be optimized for specific loading scenarios by stacking specific sequences of different infill patterns [11]. Mechanically interlocking infill has been used to improve the interface strength of multi-material parts [12]. Mustafa et al found that with significant mechanical interlocking filament the interface between the different materials approached the strength of the bulk materials [12].

The bonding of adjacent roads in polymer MEX is driven by the thermal energy of the two adjacent roads [13]. The temperature at the interface of the two roads must reach a critical temperature for the energy at the interface to reach the activation energy needed for reptation to occur [4]. The interface energy is exponentially dependent on temperature leading to an exponential incase in reptation with an increase in temperature [4]. As the interface entanglement approaches the entanglement of the bulk polymer, the interface strength approaches the strength of the bulk polymer [4]. This assumes that residual thermal stresses from cooling do not develop [4]. To maximize the time the interface between adjacent roads is above the critical activation temperature, adjacent roads should be extruded sequentially. If the adjacent roads are not printed sequentially the road extruded first would have cooled enough to significantly affect the time the interface temperature is above the critical activation temperature [6].

It has been shown that higher infill density increase the overall strength of a MEX printed part [7–9]. Higher infill density have the tradeoff of increasing the weight of the part. Contemporary slicers have the ability to change infill percentage within a part, but the slicer creates toolpaths for the different infills independently. This leads to the extruded roads at the boundaries of the different infill regions to be printed non-sequentially. The non-sequential printing of the adjacent roads leads to the road printed first being significantly cooler than the road printed second, thus inhibiting reptation [3]. This poor bonding between adjacent roads at the interface of the different infill regions drastically reduces any benefit gained from increasing the infill percentage. This work seeks to improve properties at the interface of different infill regions by considering the whole part when generating toolpaths and thus minimizing discontinuities and non-sequential printing of adjacent roads.

Methods

To determine the effect of toolpath continuity at the interface between solid and sparse infill, ASTM D638-22 type 1 4mm thick test specimens were built and loaded in tension until failure [14]. All process parameters were kept constant for all tensile test specimens with the relevant slicing parameters given in Table 1. Slic3r and Ultimaker Cura were chosen as contemporary slicers to provide baseline comparison for the novel infill combination strategies.

Table 1 Printing Parameters

Slicing Parameter	Parameter value
Extrusion Width	0.5 mm
Layer Height	0.2 mm
First Layer Printing Speed	25 mm/s
Printing Speed	60 mm/s
Infill Overlap	15%
First Layer Part Cooling Fan	0%
Part Cooling Fan	40%
Bed Temperature	60 °C
Nozzle Temperature	240 °C

Slic3r and Ultimaker Cura both have built in modifiers that were used to modify the sparse region to consist of 20% infill with the dense region consisting of 100% infill. The sparse region is centered in the gauge region and is 45mm long. Figure 1 illustrates the dense and sparse infill

region within the tensile specimen. The sparse region is shown in red and the dense regions are shown in blue. All the specimens were printed with no solid top and bottom surfaces to avoid different top and bottom surface patterns confounding the testing. The sparse and dense infill angle is +/- 45 degrees to the specimen's load axis.

Figure 1 An illustration of dense & sparse infill regions within the tensile specimen. Sparse region shown in red, dense regions shown in blue.

The novel infill combination strategies are generated using MATLAB. The MATLAB program first reads in the STL and assumes the x-y cross section is constant so only intersects the STL at one z height. The MATLAB function Polybuffer is used to generate perimeters and to define the infill regions, which allows for control of the infill overlap percentage. For the novel infill algorithm to find a continuous infill path between multiple infill regions two conditions must be met. The first condition is that the higher infill density must be collinear with the lower infill density. The second condition is that the infill travel directions must be the same along collinear paths. To guarantee these conditions the following equations define the sparse and dense infill spacing. The dense infill spacing is defined by Equation 1 and can be seen in Figure 2a.

$$Dense\ Spacing = \frac{extrusion\ width}{dense\ infill\ percentage} \quad \textbf{[1]}$$

The spacing of the spare infill lines alternates between spacing found above in Equation[1 and the spacing found below in Equation [2 and can be seen in Figure 2b.

$$Sparse\ Spacing = \frac{extrusion\ width}{sparse\ infill\ percentage} \quad \textbf{[2]}$$

This guarantees that every sparse line is collinear with a dense line thereby fulfilling the first condition listed above. This collinearity is apparent in Figure 2c. Lines with either dense or sparse spacing are generated then rotated to the desired infill angle. The lines are then intersected with their respective region boundaries to generate the intersection points on the region perimeter. These intersection points are ordered in such a way that rectilinear infill is generated. The downside of this infill generation method is the two infill densities must be odd integer multiples for the second condition listed above to be true. If the infill percentages are not odd multiples the infill lines will still be collinear, but the sparse infill will be shifted. This shift means that the tool head would be travelling in the opposite direction necessary to travel into the sparse infill from the dense infill or vice versa. Five different ways to connect the sparse and dense infill regions is explored in this paper. Illustrations of each of the build strategies used are shown in Figure 3, 4, and 5. Each color in the figures represents a single continuous toolpath.

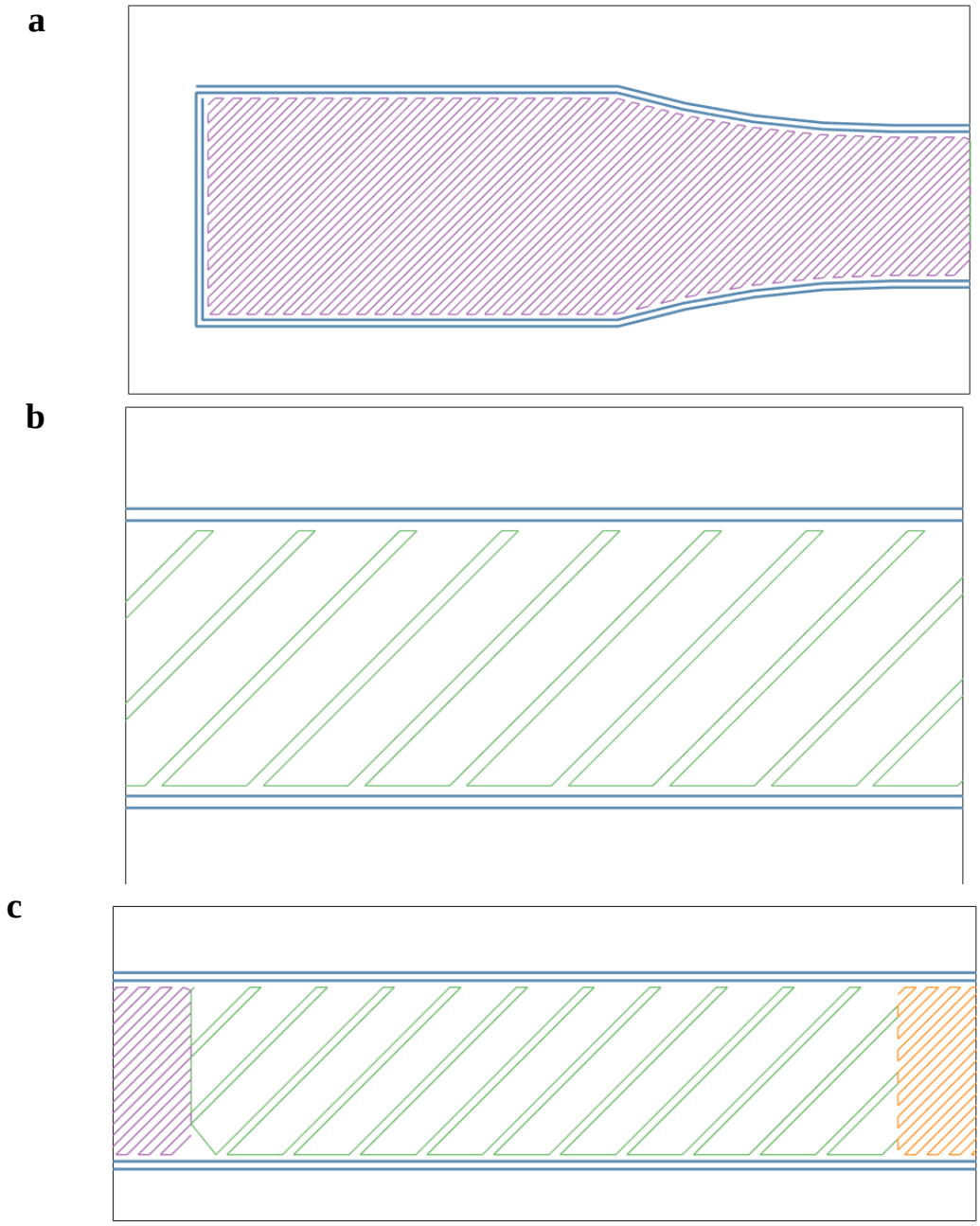

Figure 2: a) Dense infill spacing b) sparse infill spacing c) dense and sparse infill collinearity

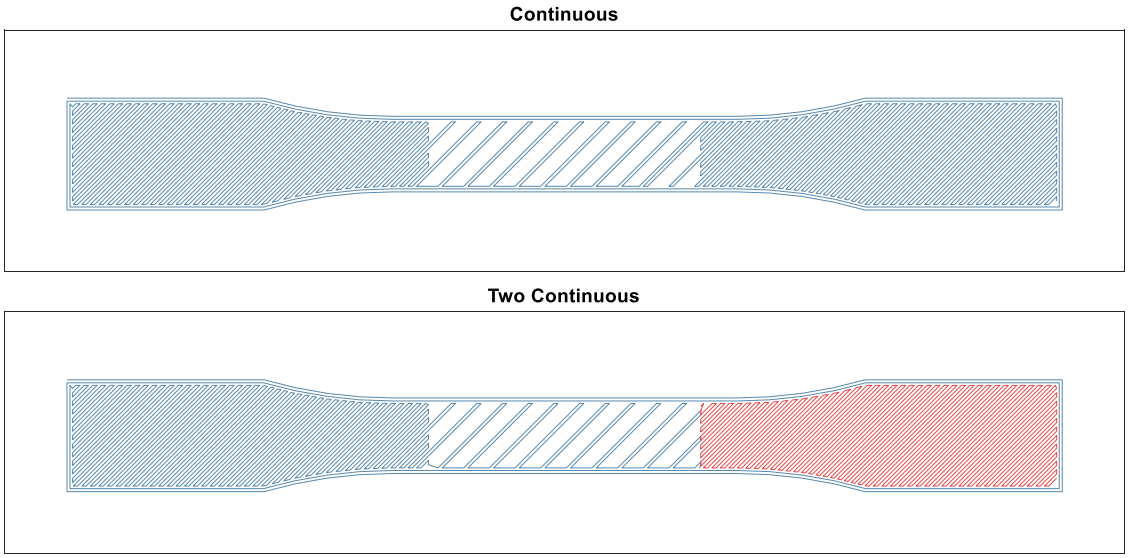

Figure 3 Continuous & Two Continuous. Each Color Represents a Continuous Toolpath

The Continuous infill combination strategy, shown in Figure 3, builds all three infill sections and the perimeters in a single continuous toolpath. The Continuous infill combination starts with the left dense region and transverses along the intersection points previously established. While traveling along the intersection points the algorithm checks if there is a sparse line collinear with the line it is traveling. If a sparse line is collinear with the current dense line the algorithm travels along the collinear sparse line instead of stopping when the dense line stops. This naturally leads it into the sparse region where it utilizes the same logic to travel back into the dense region. Travelling back is guaranteed because the sparse lines that intersect the dense-sparse boundary are collinear with a dense line and the sparse infill region is ordered such that the sparse infill travels along the bottom perimeter. The sparse infill travelling along the bottom perimeter is ideal for lining up the sparse region with the dense region, but it is not ideal for transitioning from the sparse infill region into the right dense region. The algorithm would travel into the dense region for only the lines that are collinear with the sparse region until the sparse region completely traversed. An extra road is inserted in the right side of the sparse infill to avoid the algorithm skipping a large portion of the right dense infill region. The Two Continuous strategy seen in Figure 3, avoids this extra road by traversing the sparse region completely then travelling to traverse the right dense infill region.

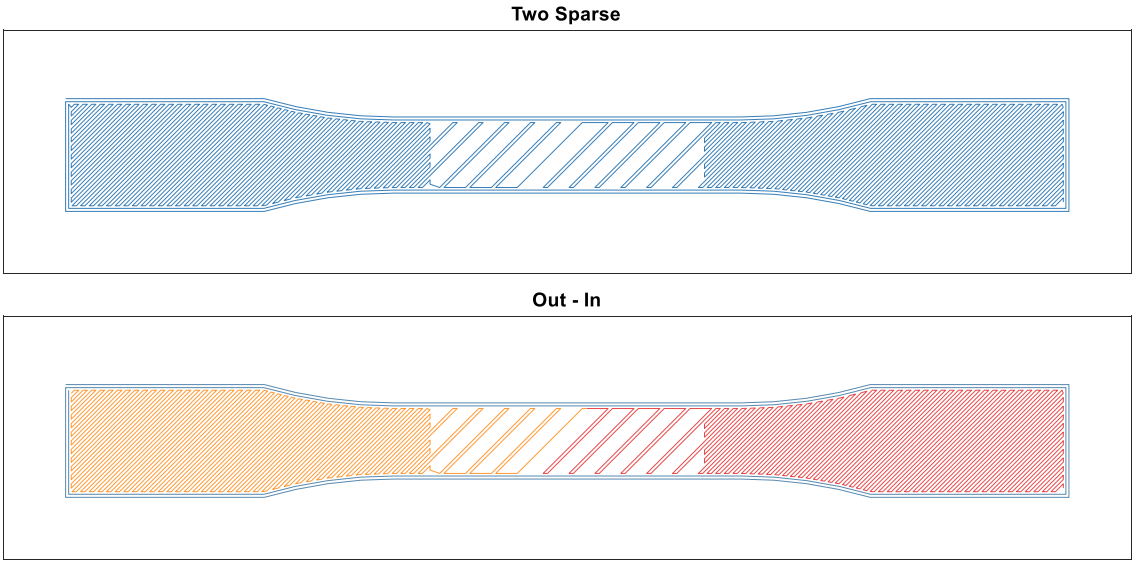

Figure 4 Weak Sparse & Out – In. Each Color Represents a Continuous Toolpath.

The Weak Sparse infill combination strategy seen in Figure 4, makes one continuous toolpath by weakening the sparse infill geometry. The sparse region travels along the bottom perimeter in the left half which allows for the smooth transition between the left dense region and the sparse region. The sparse region travels along the top perimeter in the right half which allows for the algorithm to smoothly transition into the right dense region from the sparse region without an extra road. The transition in the sparse region from traveling along the bottom to the top requires an odd number of roads. The Out – In infill combination strategy seen in Figure 4, uses the same geometry as the Weak Sparse infill combination strategy, but after extruding the left dense region and half the spares region, it then travels to the right dense region and traverses the rest of the geometry from right to left.

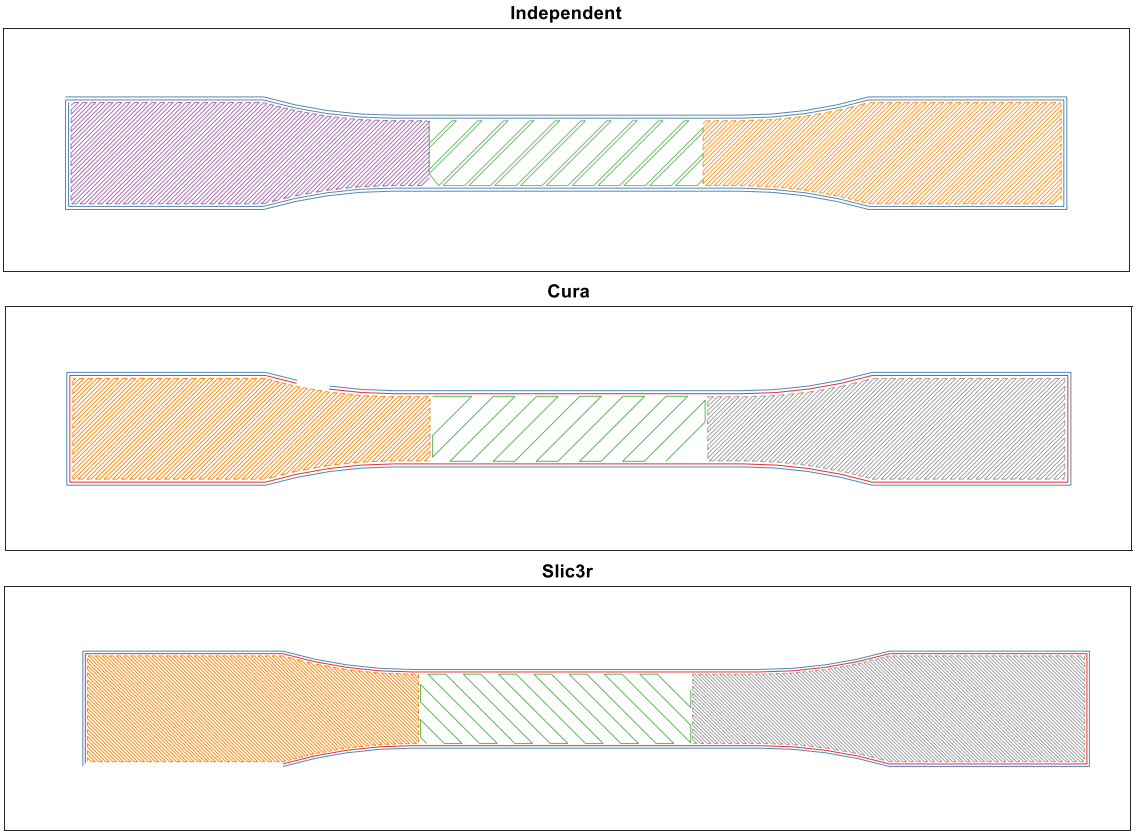

Figure 5 Independent, Cura, and Slic3r. Each Color Represents a Continuous Toolpath.

The Independent infill combination strategy starts from the left dense infill region and traverses the geometry from left to right with travel moves between each section. This infill strategy is similar to Cura and Slic3r; however, it traverses the geometry from left to right sequentially. The Cura infill combination traverse the perimeters separately, then it traverses the left dense infill region starting from the bottom right corner. After the left infill dense region is traversed it travels to the right dense infill region and traverses it starting from the top left corner. Finally it traverses the sparse infill region starting from the bottom right corner. The Slic3r similarly traverses the perimeters separately then it traverses the left dense infill region starting from the bottom left corner, then traverses the right dense infill region starting from the top right corner. Finally the Slicer infill combination traverses the sparse region starting from the top right corner.

All tensile specimens were printed using Essentium PLA XTR feedstock on a Lulzbot Mini 2.0 MEX machine. The build order of the parts was randomized to minimize outside influences affecting the builds. Tensile testing was performed using an Instron 3345 test frame equipped with a 1.5Kn load cell and BlueHill 3 control and DAQ software. 5 replications for each infill combination were tested at a strain rate of 0.1 inches per minute except for 1 specimen for the Weak Sparse infill combination which was tested at 0.2 inches per minute. The strain rate was chosen to guarantee failure occurred between half a minute and five minutes as prescribed in ASTM D638-22 [14].Effective ultimate stress was calculated according to the ASTM D638-22 standard using the dense gage region's cross-sectional geometry. The effective ultimate stress calculated does not represent the stress in the sparse region, but it allows for direct comparison

across all infill combination strategies [15]. Nominal strain was measured by dividing the change in grip separation by the original grip separation then multiplying by 100 as specified in ASTM D638-22. A one-way Analysis of Variance (ANOVA) table was calculated to compare means between infill combination categories with a significance level of 0.05. Tukey method comparisons with a significance level of 0.05 were used to compare differences in means. A one-tailed two variance hypothesis test with a significance level of 0.05 was used to compare the variances between infill combinations

Results & Discussion

To evaluate the performance of the infill combination strategies, we first discuss the tensile test results. We then perform statistical analysis on the tensile test results to prove statistical significance of mechanical properties between infill combination strategies. Finally we discuss observations from the tensile testing including fracture characteristics of the different infill combination strategies.

The average effective ultimate stress and average nominal strain at break results from testing 5 replications of each infill combination strategy are shown in Table 2. Yield stress was not recorded due to all specimens demonstrating brittle failure. The average effective ultimate stress for Cura and Slic3r is lower than every other infill combination strategy. Similarly the average nominal strain at break for Cura and Slic3r is lower than every other infill combination strategy.

Table 2 Tensile Test Results

Infill Combination Strategy	Average Effective Ultimate Stress [MPa]	Average Nominal Strain at Break [%]
Weak Sparse	9.60 (0.94)	1.62 (0.13)
Slic3r	8.01 (0.56)	1.51 (0.063)
Independent	8.94 (1.4)	1.87 (0.17)
Out – In	8.69 (0.52)	1.69 (0.12)
Cura	7.98 (1.5)	1.59 (0.11)
Continuous	9.16 (0.79)	2.01 (0.80)
2 Continuous	8.61 (1.6)	1.93 (0.20)

Standard deviations are listed in parenthesis

A one-way ANOVA test to compare the mean effective ultimate stress of the infill combination strategies was performed. We found that at a 5% significance level we do not have enough evidence to claim a difference in mean effective ultimate strength for at least one of the infill combination strategies. This claim is apparent when looking at Figure 6 as every boxplot overlaps every other boxplot. One proposed benefit of a continuous toolpath is a reduction in defects, leading to more consistent parts. The standard deviation of the continuous infill combination strategy is smaller than the standard deviation of the Cura infill combination strategy, but the Slic3r infill combination strategy has a lower standard deviation then both Continuous and Cura. The variation in the MEX AM process leads to a wide range of as built mechanical properties, such that only drastic changes in mechanical properties can be proven statistically significant.

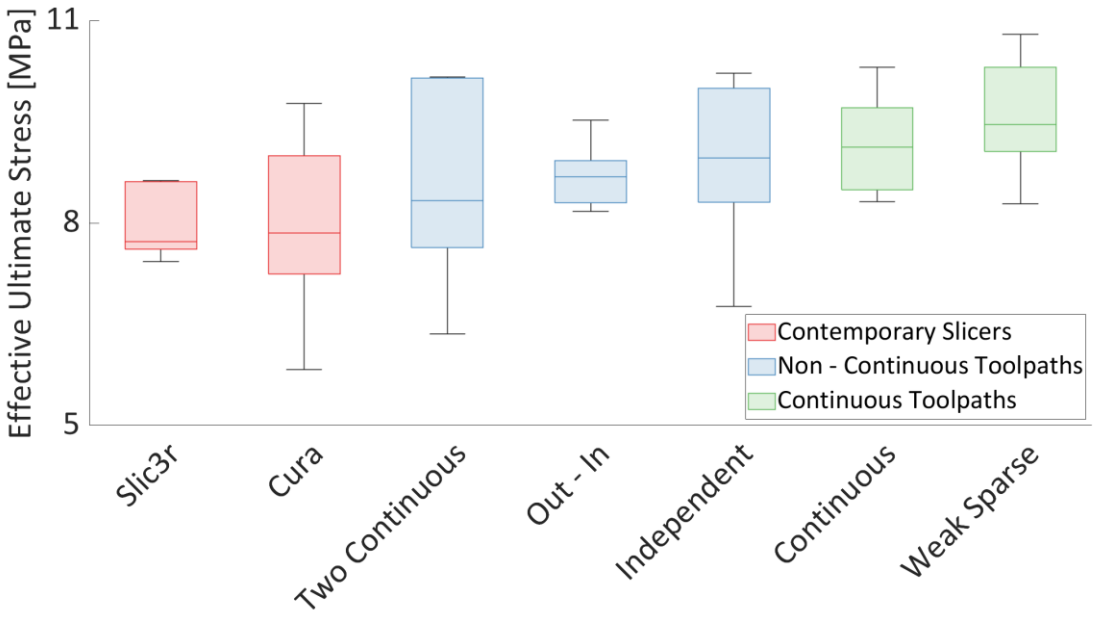

Figure 6 Effective Ultimate Stress Boxplots

A one-way ANOVA test to compare the mean nominal strain at break for the various infill strategies was performed. We found that at a 5% significance level we have enough evidence to claim that at least one of the infill combination strategies has a different mean nominal strain from at least one other infill combination strategy. The boxplots in Figure 7 showcase this difference in mean nominal strain between the infill combination strategies. Tukey method comparisons at a 5% significance level were carried out to evaluate differences in nominal strain at break true means. Table 3 showcases the results of the Tukey method simulations. From the Tukey method comparisons we can claim that Continuous, 2 Continuous, and the Independent infill combination strategies have a higher true mean nominal strain at break than Cura and Slic3r.

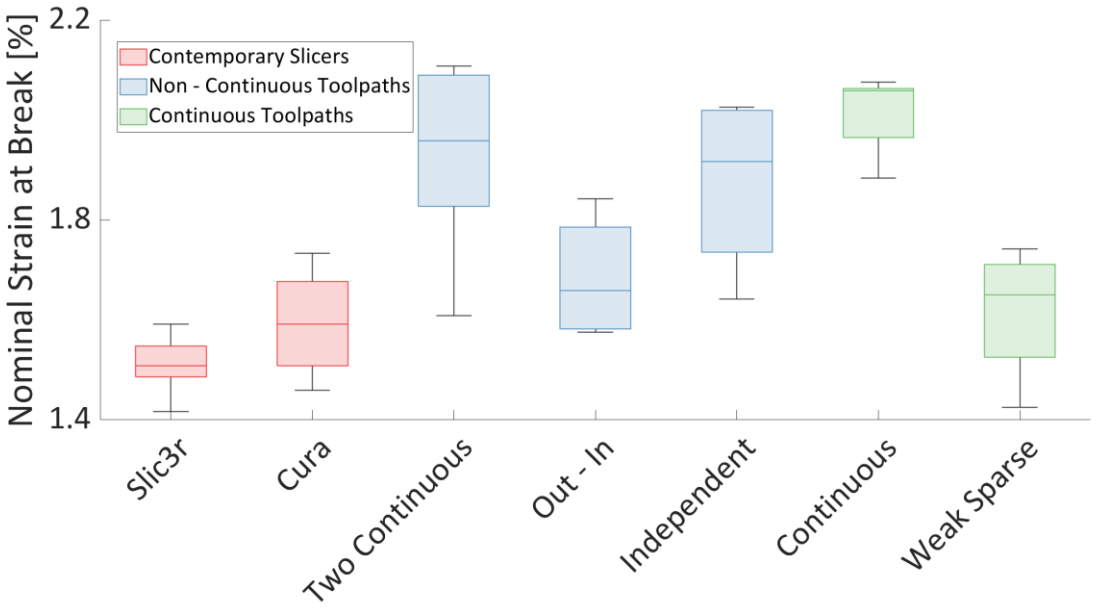

Figure 7 Nominal Strain At Break Boxplot

Table 3 Nominal Strain at break Tukey Method Comparison Results

Infill combination Strategy	Mean	Grouping			
Continuous	2.01	A			
2 Continuous	1.93	A	B		
Independent	1.87	A	B	C	
Out – In	1.69		B	C	D
Weak Sparse	1.62			C	D
Cura	1.59				D
Slic3r	1.51				D

Means that do not share a letter are significantly different

Infill combination strategies that displayed a statistically significant higher nominal strain at break (those that belong to group A), break in approximately the center of the gage region. Out – In and Weak Sparse consistently break in known weak-points in the geometry, the single road for Weak Sparse and the discontinuity point in Out – In. The Cura and Slic3r test specimens broke at a variety of locations, indicating that these infill combination strategies suffered from defects. Specimens produced using Cura showcased brittle fracture of the sparse infill region from the perimeters throughout loading as can be seen in Figure 8. Slic3r specimens frequently broke along one perimeter first leading to the warped sparse infill section seen in Figure 8.

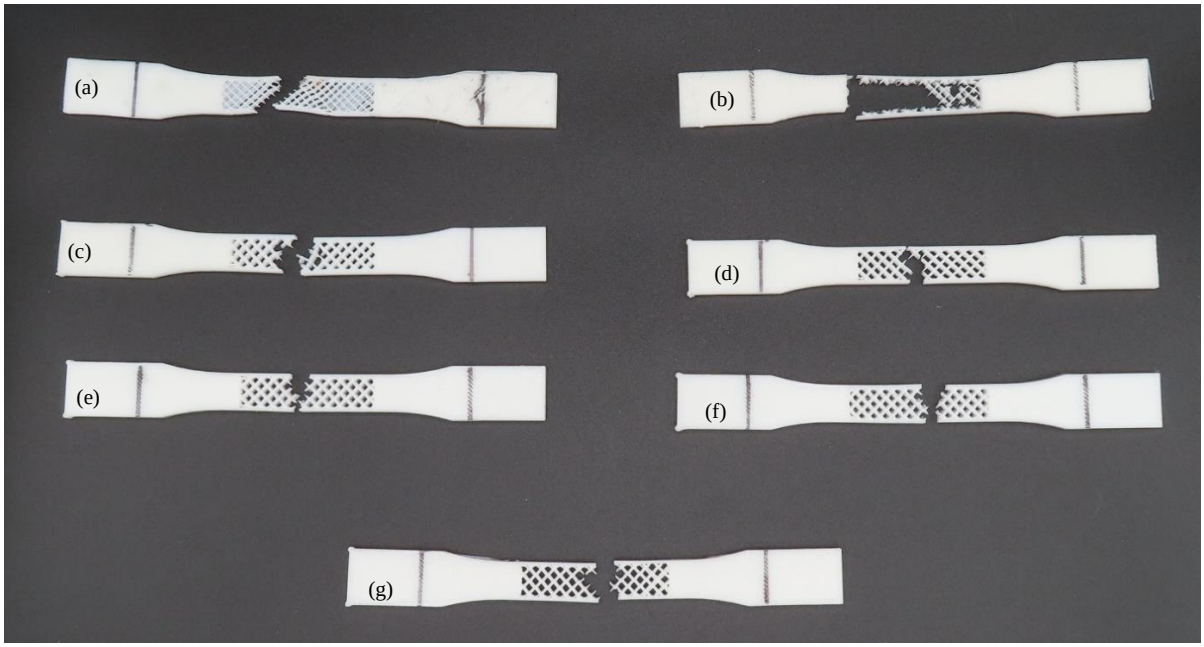

Figure 8 Representative Failed Tensile Specimens
(a) Slic3r (b) Cura (c) Out – In (d) Weak Sparse (e) 2 Continuous (f) Independent (g) Continuous

Slic3r specimen's multi-stage fracture is apparent when looking at Figure 9. The Slic3r specimens appear to be fracturing at defects with a significantly lower nominal strain than expected. The other portions of the specimen continue to resist load to a larger nominal strain. The statistically significant lower nominal strain along with the observations of the failure behavior both point to Slic3r and Cura infill combination strategies having significantly more defects than the more continuous toolpaths.

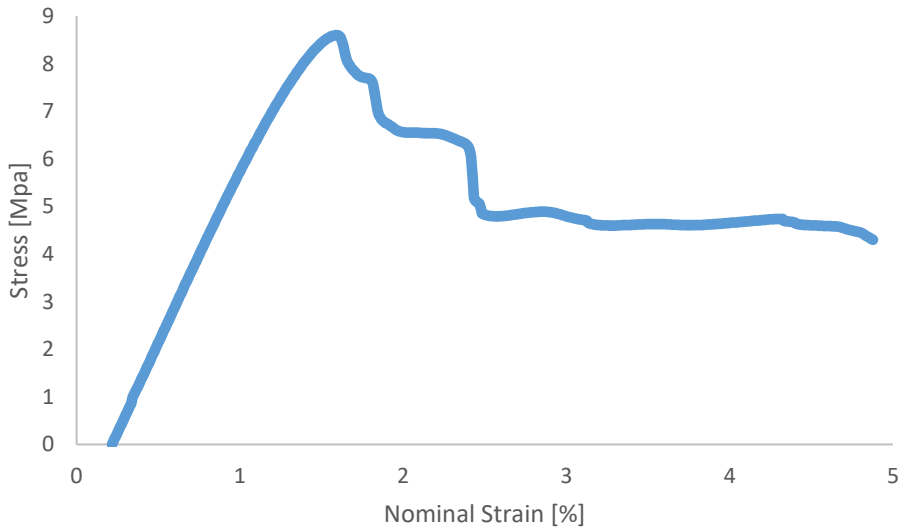

Figure 9 Slic3r Stress vs Strain curve

The Independent infill combination strategy performed better then Out – In and Weak Sparse even though it has more discontinuities. The Independent infill combination strategy has a

similar number of toolpaths as Cura but the roads are printed sequentially from left to right unlike in Cura. The difference in the order of the toolpaths can be seen in Figure 10. This suggests that the poor bonding in discontinuous adjacent roads are diminished if the adjacent roads are sequentially extruded. The sequentially extruded roads have the least amount of time to cool before an adjacent road is placed leading to the interface between the roads maintaining the critical temperature for reptation for longer. The good mechanical properties of the Independent infill combination strategy suggests that discontinuities are preferable to the single roads found in Weak Sparse and Out – In as long as the discontinuous paths extruded adjacent roads sequentially. Two Continuous has a statistically significant greater average nominal strain at break than Weak Sparse, providing more proof. The large standard deviation for the Independent infill combination strategy is possibly due to increase chance of defects at toolpath discontinuities, further complicating finding an optimal toolpath.

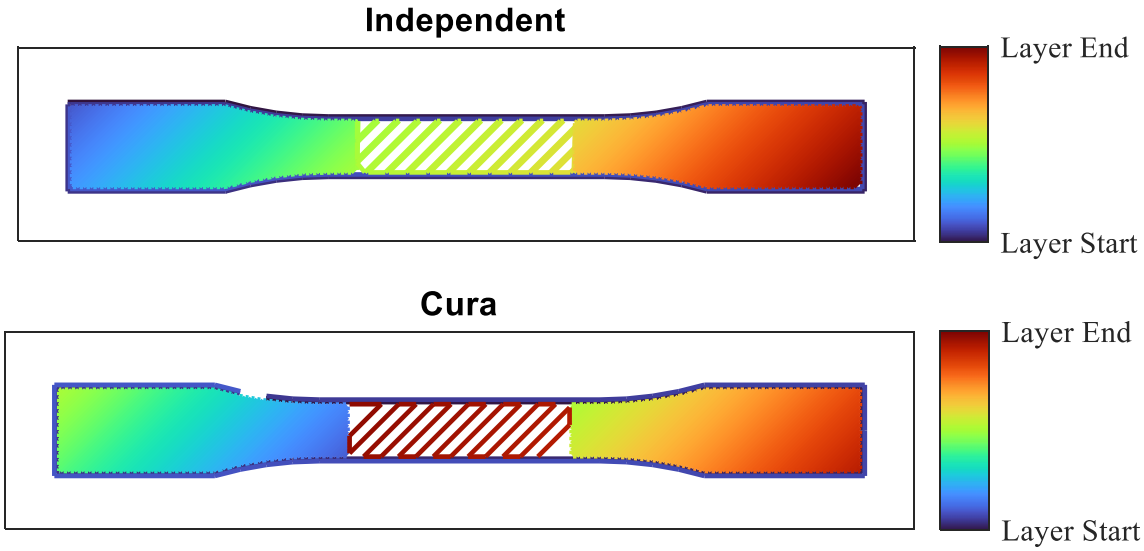

Figure 10 Independent & Cura Print Order

Conclusion & Future Work

Novel infill combination strategies were tested for MEX AM that minimized discontinuities, to reduce defects and increase mechanical properties. Novel infill combinations along with specimens built with contemporary slicers were compared using tensile testing. Continuous toolpaths showcased better mechanical properties than the discontinuous toolpaths generated by contemporary slicers. Sequentially printing adjacent roads regardless if they are continuous is preferable to forcing a continuous toolpath by weakening the geometry.

The algorithms presented in this paper are extremely narrow in scope and cannot easily be generalized to other geometries or other infill patterns. The algorithm's runtime scales poorly with an increase in toolpath points, i.e. Increase in infill density or an increase in area to fill. For these reasons the author's current work abandons these algorithms and is using graph theory to robustly generate continuous and spatially aware toolpaths for polymer MEX AM systems. A slicer agnostic tool that modifies Gcode to sequentially print infill sections has been motivated by the conclusions of this work.

References

[1] How to Adjust Print Settings of a Part of My Model in Ultimaker Cura. https://support.makerbot.com/s/article/1667417981430. Accessed May 18, 2023.

[2] Slic3r Manual – Welcome to the Slic3r Manual. https://manual.slic3r.org/. Accessed May 18, 2023.

[3] Joseph Bartolai. *Predicting and Improving Mechanical Strength of Thermoplastic Polymer Parts Produced by Material Extrusion Additive Manufacturing*. The Pennslyvania State University.

[4] Grewell, D., and Benatar, A. "Welding of Plastics: Fundamentals and New Developments." *International Polymer Processing*, Vol. 22, No. 1, 2007, pp. 43–60. https://doi.org/10.3139/217.0051.

[5] Roy, M., Yavari, R., Zhou, C., Wodo, O., and Rao, P. "Prediction and Experimental Validation of Part Thermal History in the Fused Filament Fabrication Additive Manufacturing Process." *Journal of Manufacturing Science and Engineering*, Vol. 141, No. 12, 2019, p. 121001. https://doi.org/10.1115/1.4045056.

[6] Thomas, R. "Modeling the Fracture Strength Between Fused-Deposition Extruded Roads."

[7] Abbas, D. T., Othman, D. F. M., and Ali, H. B. "Effect of Infill Parameter on Compression Property in FDM Process." Vol. 7, No. 10, 2017.

[8] Yadav, P., Sahai, A., and Sharma, R. S. "Strength and Surface Characteristics of FDM-Based 3D Printed PLA Parts for Multiple Infill Design Patterns." *Journal of The Institution of Engineers (India): Series C*, Vol. 102, No. 1, 2021, pp. 197–207. https://doi.org/10.1007/s40032-020-00625-z.

[9] Pandzic, A., Hodzic, D., and Milovanovic, A. Effect of Infill Type and Density on Tensile Properties of PLA Material for FDM Process. In *DAAAM Proceedings* (B. Katalinic, ed.), DAAAM International Vienna, 2019, pp. 0545–0554.

[10] Naik, M., Thakur, D. G., and Chandel, S. "An Insight into the Effect of Printing Orientation on Tensile Strength of Multi-Infill Pattern 3D Printed Specimen: Experimental Study." *Materials Today: Proceedings*, Vol. 62, 2022, pp. 7391–7395. https://doi.org/10.1016/j.matpr.2022.02.305.

[11] Dave, H. K., Patel, B. H., Rajpurohit, S. R., Prajapati, A. R., and Nedelcu, D. "Effect of Multi-Infill Patterns on Tensile Behavior of FDM Printed Parts." *Journal of the Brazilian Society of Mechanical Sciences and Engineering*, Vol. 43, No. 1, 2021, p. 23. https://doi.org/10.1007/s40430-020-02742-3.

[12] Mustafa, I., and Kwok, T.-H. "Development of Intertwined Infills to Improve Multi-Material Interfacial Bond Strength." *Journal of Manufacturing Science and Engineering*, Vol. 144, No. 3, 2022, p. 031009. https://doi.org/10.1115/1.4051884.

[13] Li, L., Sun, Q., Bellehumeur, C., and Gu, P. "Investigation of Bond Formation in FDM Process."

[14] D20 Committee. *Test Method for Tensile Properties of Plastics*. ASTM International.

[15] Bartolai, J., Wilson-Heid, A. E., Kruse, J. R., Beese, A. M., and Simpson, T. W. "Full Field Strain Measurement of Material Extrusion Additive Manufacturing Parts with Solid and Sparse Infill Geometries." *JOM*, Vol. 71, No. 3, 2019, pp. 871–879. https://doi.org/10.1007/s11837-018-3217-1.